05

Superconducting RF Passing Power Detector (SPPD)

© E.R. Khan,[1] N.Yu. Rudenko,[1] V.I. Chichkov,[1] S.V. Shitov[1,2]

[1] National University of Science and Technology MISiS,
119049 Moscow, Russia
[2] Kotelnikov Institute of Radio Engineering and Electronics, Russian Academy of Sciences,
125009 Moscow, Russia
e-mail: inlovewithfaraday@gmail.com, sergey3e@gmail.com

Received May 14, 2025
Revised May 14, 2025
Accepted May 14, 2025

This paper describes the development and experimental study of an original superconducting microwave (MW) throughput signal detector based on RFTES technology, designed for measuring ultra-weak signals in the microwave frequency range from 1 to 40 GHz and potentially beyond. The device utilizes thin-film superconducting microbridges operating near their critical temperature, enabling high sensitivity to throughput signal power at levels of the order of 10^{-13} W and an insertion loss of less than -30 dB. The detector is implemented as a planar integrated structure, making it suitable for cryogenic applications, including integration into superconducting quantum devices such as qubits, parametric amplifiers, and frequency mixers. Key advantages of the detector include its broad operational frequency range and compatibility with complex superconducting circuits. The paper presents details on the device's structure, fabrication parameters, and preliminary results of the experimental study of the detector based on niobium and hafnium thin films. The comparison of simulated and measured S-parameters of experimental samples at frequencies of most interest around 1.5 and 7 GHz, at temperatures around 100 mK, are provided.

Keywords: RFTES bolometer, superconducting resonator, integrated planar structure.

DOI: 10.61011/TP.2025.09.61842.101-25

Introduction

Superconducting microwave detectors have firmly occupied key positions in modern technologies related to the processing and measurement of ultra-weak signals, in applications such as observational astronomy, radiometry, and microwave metrology [1–4]. In recent years, considerable attention has been paid to the development of detectors capable of operating at ultra-low temperatures, which can play an important role in the field of creating quantum computers using superconducting qubits and parametric amplifiers. A relevant option is detectors of transmitted power, the function of which is to measure signals passing through the microwave transmission line, and such measurement should be as non-invasive as possible, i.e. there is no effect on the passage of such signals. It should be noted that existing solutions, such as semiconductor detectors in combination with directional couplers, have limited sensitivity and are not always suitable for integration into a system operating at ultra-low temperatures, especially in superconducting integrated circuits.

The motivation for this research is the idea of creating a transmitted signal detector that takes advantage of the new technology of RFTES detectors [5]. The purpose of the transmitted power detector is to measure the signal with negligible energy extraction from the signal path. In the future, this detector can form the basis of an integrated structure with a detector and a superconducting qubit on a single chip for non-invasive registration of the qubit state. Similar studies have been actively conducted by various scientific groups in recent years. A bolometer based on a resistive nanowire in combination with Josephson junctions has already been tested for this purpose [6]. A microwave photon counter based on a parametric amplifier was used in Ref. [7] to measure the state of a superconducting qubit. Non-destructive signal detection was achieved due to the weak coupling of the detector with the qubit, which made it possible to measure photons without direct absorption of energy from the quantum system. The solutions proposed today do not represent a single integrated device, which leads to a number of technical difficulties, the need for complex calibration, affecting the efficiency of the interface between the qubit and the detector and, as a result, to insufficient reading reliability. Successful studies of other superconducting detectors capable of detecting signals in the terahertz range are known, for example, TES bolometers and MKID detectors, but their use for measuring microwave signals in the relatively low frequency range of 1–40 GHz remains limited to this day [8–10]. One of the closest analogues of our proposed solution is the uncooled detector described in Ref. [11], which uses semiconductor diode detectors. It is clear that such uncooled devices have limited sensitivity, their optimization for operation in cryogenic conditions is a difficult engineering and physical task, and they are definitely not suitable for use in superconducting integrated circuits.

The device described below is one of the promising solutions to overcome the existing difficulties of integrating

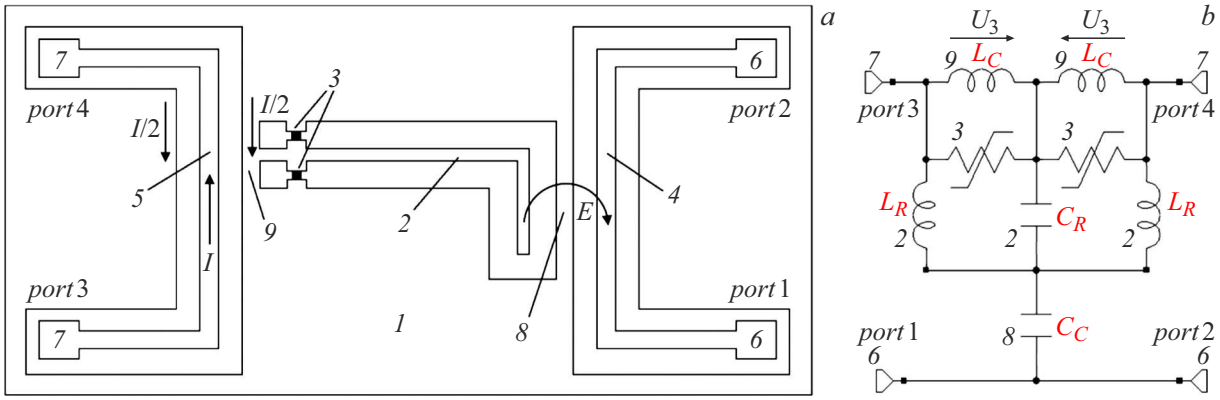

Figure 1. Conceptual topological scheme of a superconducting microwave detector of transmitted power (*a*) and its simplified equivalent electrical circuit (*b*): *1* — dielectric substrate coated with a superconducting film; *2* — quarter-wave coplanar resonator loaded with superconducting bridges; *3* — superconducting bridges; *4* — resonator excitation line *2* in which |S21| is measured; *5* — line of the transmitted microwave signal; *6* — ports of the resonator excitation line; *7* — ports of the transmitted microwave signal line; *8* — section of the capacitive coupling of the resonator *2* and the reading line *4*; *9* — inductor coupling of superconducting bridges with microwave signal current in the line *5*; U_3 — voltage drop across the bridges *3*; L_R — resonator inductance, C_R — resonator capacitance, L_C — coupling inductance, C_C — coupling capacitance. The local microwave grounding is not shown (*b*). Port 1–4 — designation of ports in calculations. The arrows indicate the current directions in the coplanar waveguide. The arc marks the antinode area of the electric field.

a sensor for the state of a superconducting qubit on the same substrate with the qubit itself. It is based on an L-type RFTES detector, or an RFTES detector with inductive coupling to a resonator, the role of which is performed by an inductive shunt [12]. Such a detector can be integrated into the general manufacturing process of a qubit. The relevance of the presented research is due to the current trend towards finding ways to create a compact and highly sensitive sensor in the ~ 10 GHz band capable of measuring ultra-low signal strengths in a wide microwave range and suitable for integration into superconducting circuits, including quantum signal processing circuits.

1. Structure and operating principle of the detector

The studied transmission power detector is an integrated planar thin-film superconducting structure (chip) on a dielectric substrate with four terminals: two for the input and output of the transmission line of the measured microwave signal and the other two for the input and output of the resonator excitation line and the reading of the RFTES detector. Fig. 1, *a* shows a schematic representation of the detector topology.

The detector includes a dielectric substrate *1* coated with a niobium film as a microwave shield in which the remaining elements of the device are formed. The resonator *2* is made in the form of a quarter-wave segment of a coplanar waveguide connected to the excitation (readout) line *4* via capacitive coupling *8*. The resonator is loaded with thermoresistive bridges *3* made of a thin superconducting hafnium film, which are connected in parallel to two parts of the inductor *9*, symmetrical with respect to the central part of the resonator. The inductor determines the current transfer coefficient from the measured signal line *5* to the bridges. The excitation (reading) line and the measured signal line have contact pads *6* and *7*, respectively.

The monochromatic reading signal (carrier) is applied through the contacts *6* lines *4* and excites the resonator *2* in the field of capacitive coupling *8*. The resonator current flows through bridges *3* and heats up the electronic subsystem in the superconducting hafnium film to an operating temperature near the temperature of the superconducting transition, where a sharp change in the active resistance is observed under the influence of heat, and the Q-factor of the resonator changes. The resonator is connected in such a way that it provides a dip in the amplitude-frequency response of the reading line *4* at the resonator frequency. The depth of such a dip depends on the total heating current of the bridge, and, thus, is a measure of the sum of the heating power from the resonator and the microwave signal passing through the line *5*.

Let us briefly discuss the principle of operation of the RFTES detector. Such a detector uses the region of dependence of the superconductor resistance on temperature near the temperature of the superconducting junction at $R(T) \approx 0.1R_n$. This is reflected in the abbreviation TES in the name of the RFTES technology as a reference to TES detectors operating in the same operating resistance range of the superconducting film. The fundamental difference lies in the method of signal absorption and registration of the variation $R(T)$ resulting from the heating of the absorber by the input signal: instead of the thermal contact of the superconducting TES thermometer with the areal absorber in the RFTES detector, the current of the THz signal and the microwave reading current are fed directly into the thermometer circuit, warming it up. Thus, instead

of the direct (low-frequency) current used in TES detectors, radio-frequency (RF) current is used, which determines the full name of the detector (its construction technology) — RFTES. The reading of such a thermometer is carried out indirectly through a change in the Q-factor of the microwave resonator, which changes its Q-factor when the resistance of the bridge thermometer changes under the influence of the measured signal. It is known that a high Q-factor superconducting quarter-wave resonator at a resonant frequency suppresses the passage of a signal along the excitation line between contacts *6–6* (Fig. 1) in proportion to its loaded Q-factor.

The resonator is also connected to the excitation line in the studied device, and variations in its Q-factor lead to modulation of the carrier power, which is recorded using standard methods based on measuring S-parameters, as a result of which a dip appears in the transmission spectrum of the excitation line, the minimum transmission coefficient |S21(F)|. The previously tested terahertz RFTES detectors received a signal from a well-matched planar antenna, and the new solution uses galvanic contact and obviously poor coupling with a relatively low-frequency signal line. Thanks to the Andreev reflection effect (in other words, creating Andreev mirrors for quasiparticles) at the boundary of the hafnium bridges with the niobium electrodes, a regime of trapped hot electron gas is realized. The Andreev reflection effect persists up to frequencies on the order of the gap frequency of niobium, i.e., up to ~ 750 GHz. A similar thermal insulation can occur in the case of a dielectric non-tunnel (oxide) layer at the boundaries of the bridge, which also creates an insurmountable obstacle for any current carriers. The isolation efficiency of a hot electron gas in an RFTES detector was measured experimentally at a resonator reading frequency of 1.5 GHz and described in [13].

The combination of hafnium and niobium materials allows measurements to be carried out over a wide temperature range, in particular at 130 mK. A special feature of hafnium is the low density of states at the Fermi level, the low level of electron-phonon interaction, which slows down the transfer of heat from electrons to the lattice. This makes it possible to concentrate thermal energy mainly in the electronic subsystem, thus realizing the thermal insulation of the electronic „absorber“ relative to the lattice and substrate, which is important for improving the sensitivity of any bolometric (thermal) detector. In this case, the electrons thermalize (acquire the same heating) relatively quickly, $\sim 0.1\,\mu$s at a temperature of 400 mK, and cool through the lattice two orders of magnitude slower, $\sim 10\,\mu$s [14]. The different time of electron thermalization and complete thermalization of the film is nonequilibrium heating. At the same time, the lattice remains „cold“ to a first approximation.

The integrated RFTES detector absorber based on a hafnium film in combination with an inductive shunt has a low impedance, and therefore is weakly connected to the measured signal line, taking a very small part of the power (about -30 dB). The possibility of detection in the transmitted power mode is due to the high sensitivity of the RFTES detector with the effect of heating the electron gas with microwave current (noise-equivalent power) NEP $\sim 10^{-17}$ W/$\sqrt{\text{Hz}}$ [5]. Such a detector can be used at signal levels of -100 dBm in a wide frequency range of the measured signal, from 1 to 40 GHz, according to the estimates. A special feature of the new device is a balanced scheme for suppressing the carrier power (reading signal) of the RFTES detector, which is important for its further integration with qubits that are sensitive even to a relatively small number of photons of extraneous signals.

An equivalent electrical circuit of a superconducting microwave detector of transmitted power is shown in Fig. 1, *b*, the numbers correspond to the numbers in Fig. 1, *a*. A coplanar resonator is described by a capacitance C_R and inductors L_R (~ 1 nH) (these elements are marked with a number *2*). The resonator is loaded with bridges *3* with a resistance in the operating range of the order of $0.1R_n$, where R_n is the resistance in the normal state. The bridges are connected parallel to the shunts L_C (~ 10 pH) *9*. The resonator is excited through the coupling capacitance *8*.

The loaded Q-factor of the resonator is determined by the active resistance of the bridges connected to the resonator current circuit parallel to each half of the inductor near the shorted end of the resonator. Such bridges, according to RFTES technology, act as thermistors, i.e. elements with active nonlinear impedance $R(T) = \text{Re}(Z(T))$. By selecting the power of the excitation signal (carrier power), the electronic subsystem in the bridge film is heated by the resonator current, which makes it possible to set their impedance to the working area with the highest sensitivity of the transmission coefficient |S21(F,T)| to the variation in the heating power introduced by the measured signal, which means the maximum value of the function $dR(T)/dT$.

A coplanar waveguide as an ideal electrodynamic system is formed by the following conductive surfaces: a central line (strip) symmetrically located in the gap between semi-infinite conducting planes (grounds). The current distribution of such a waveguide is described by the current of the central line (strip) and two parallel currents of the opposite direction, return currents flowing along the edges of the conducting planes (along the edges of the grounds), each of which is equal to half the current of the central strip. Such a classical structure of coplanar waveguide currents imposes boundary conditions in the region *8* at the open end of the resonator *2* — there is no resonator current there either in the strip or in the banks, regardless of whether current flows in the excitation line *4*. Thus, in the region of the open end of the coplanar waveguide, an electric field antinode is formed at the resonance frequency, which is enhanced due to the high Q-factor of the resonator ($Q \sim 10^4$). Most of the electric field is drawn into the dielectric substrate and forms a substantial electrical capacitance with the surrounding surfaces, including the central strip *4*. The coupling element *8* negatively affects the coupling *4–2*, since it is part of the shielding metal, but cannot be excluded from the electrodynamic circuit, since

it is responsible for maintaining the symmetry of the return currents of the coplanar waveguide *4*. Thus, the inductive coupling with the resonator in the area of the element *8* is extremely inefficient, and the coupling of the resonator with the excitation line occurs due to a strong electric field, i.e. it has a capacitive character. The structure of the currents of a coplanar waveguide in the area of element coupling *7* and *3* are such that half of the return current of the strip *5* $(I/2)$ passes through the section *9*, and part of this current flows into the bridges *3*, which has an equivalent circuit with galvanic coupling, as shown in Fig. 1, *b*.

The size of the bridges is less than $10\,\mu$m, which is three to four orders of magnitude smaller than the wavelength of the signal used, and the intensity of extraneous modes in the signal waveguide caused by the asymmetry of coplanar currents cannot exceed the power taken from the main mode. Contact pads are surrounded by metal in Fig. 1, *a*, which works in the same way as bridges used to suppress the parasitic slot mode of a coplanar waveguide. A slot mode can also occur in the detector's coplanar quarter-wave resonator, but under existing boundary conditions, its resonant frequency is twice as high, and this cannot affect the detector's operation.

The power loss of the measured signal at the active resistance of the bridges $R(T)$ *3* is determined by the current in the signal transmission line and the impedance of the shunt inductors X_L *9*, which is designated as the coupling inductance L_C. When the bridges and inductors are switched on connected in parallel, an increase in the impedance of the bridge caused by heating from the signal causes an increase in the current flowing through the inductive shunt. Thus, the reactive current in the detector resonator increases, and the Q factor increases, causing an increase in the dip of the parameter $S21(F)$, which is easy to measure. A more detailed consideration can be carried out by calculating the effective value of the active bridge impedance R_e as a function of the heating temperature and frequency. To do this, it is convenient to use the concept of the reactive bypass coefficient Γ, which is inversely proportional to the quality of the shunt:

$$\Gamma = Q^{-1} = (\omega L/R)^{-1} = R/\omega L. \tag{1}$$

It is easy to show that the real and imaginary parts of the impedance Z of a circuit consisting of a parallel-connected resistor R and a reactive shunt $|X|$ can be calculated using the following simple and useful ratios that transform the complex conductivity of a parallel circuit multiple elements in a complex impedance. Such a conversion implies the complete equivalence of the „recalculated“ circuit, in which the signal current flows sequentially through the modified values of the resistor and the reactive element:

$$\mathrm{Re}(Z) = \frac{R}{1+\Gamma^2}, \tag{2}$$

$$|\mathrm{Im}(Z)| = \frac{|X|\Gamma^2}{1+\Gamma^2}, \tag{3}$$

$$\frac{\mathrm{Re}(Z)}{|\mathrm{Im}(Z)|} = \frac{R}{|X|\Gamma^2} = \Gamma^{-1}. \tag{4}$$

The module is specified for the reactive part of the impedance Z, since the sign of the complex impedance will be different for the capacitive and inductive shunt. It is important that the above expressions can be used for both inductive and capacitive shunts. These expressions make it easy to calculate the losses introduced into the resonator. It should be noted that the ratio of the modified impedances (4) remained the same as for the conductivities. In addition to this, it can be noted that the reactive component of the impedance dominates the circuit, and it is the symmetry of the inductors, rather than the resistances of the bridges, that determines the balance (mutual compensation) of the detector resonator currents introduced into the waveguide of the transmitted signal.

In our case, the optimal impedance of one bridge is $R(T) \approx 3\,\Omega$, and the shunt inductance is $L = 4\,$pH, which gives $|X_L(F)| \approx 0.17\,\Omega$ at a frequency of $\sim 7\,$GHz, and the active resistance in the signal current circuit it will be $R_e \approx 0.01\,\Omega$. It should be noted that this value will depend on the frequency, and in the case of an inductive shunt, it increases, and our detector requires frequency calibration. The absorption coefficient in the case of a strong load mismatch can be written using the well-known formula for matching two active impedances as

$$C_A(Z_1, Z_2) = \frac{4\mathrm{Re}(Z_1)\mathrm{Re}(Z_2)}{(\mathrm{Re}(Z_1)+\mathrm{Re}(Z_2))^2 + (\mathrm{Im}(Z_1)+\mathrm{Im}(Z_2))^2},$$

$$C_A(R_e, 50) = \frac{4(50\cdot 2)2R_e(F)}{(50\cdot 2 + 2R_e(F))^2}\cdot 0.5 \approx 2\,\frac{2R_e(F)}{(50\cdot 2}$$

$$= \frac{2R_e(F)}{50} = 4\cdot 10^{-4} \approx -34\,\mathrm{dB}.$$

The final result is written in the approximation $R_e \ll 50\,\Omega$, and the expression is reduced to $4R_e(F)/(50\cdot 2)$, which takes into account that the detector contains two symmetrical absorbers and is symmetrically connected to two ports of the signal line, which results in a coefficient of $1/2$. Approximately, the insertion loss can be estimated as very small (about -30–$40\,$dB), which means that the detector has a negligible effect on the measured signal. Using the above values, we obtain that $\Gamma = Q^{-1} \approx 17$ at a frequency of $7\,$GHz. An estimate at a frequency of $40\,$GHz gives $\Gamma \approx 3$, $R_e \approx 0.3\,\Omega$, and the insertion loss will increase to $\approx -19\,$dB from the incoming signal, which is equivalent to $1.2\,\%$, or a decrease in transmitted power by $0.052\,$dB, that should also be considered a negligible value, which is below the level of the typical error in measuring microwave power. A special frequency range is the frequencies in the immediate vicinity and below the pump frequency of the detector. Near the pumping frequency, the signal and the carrier can beat if these frequencies differ by less than a resonator band, typically — less than 1 MHz. The bridge warming effect

can degrade at the lowest frequencies, due to the low energy of the signal photons.

In summary, variations in the power of the transmitted signal change the degree of heating of the bridges and their impedance, which leads to a change in the Q-factor of the resonator and is recorded by measuring the modulus of the transmission coefficient $|S21(F)|$ of excitation line of the detector. Due to the symmetric connection of identical bridges to the waveguide, the voltages induced on them by the detector resonator current are subtracted and do not create a current in the signal waveguide. That is, within the lumped-element circuit approximation (Fig. 1, *b*), they do not transfer a signal at the readout frequency into the signal waveguide. Such a connection can be classified as a balanced circuit. It is important to note that when registering a signal, the resonator does not change its resonant frequency, since the impedance of the bridges is dominated by the variation of the active impedance, which follows from the analysis of the ratio (3) for $\Gamma \gg 1$: the reactive component changes little, which means that a small change in the active resistance of the bridges practically does not affect the resonator frequency.

2. Detector manufacturing

Thermoresistive bridges are made of 80 nm thick superconducting hafnium film and have an active region size of $1 \times 1\,\mu$m. Part of the bridge film is covered with niobium electrodes with a thickness of 100 nm. The choice of materials is determined by their superconducting properties at cryogenic temperatures (critical temperature of a thin hafnium film $T_{c\mathrm{Hf}} \approx 400$ mK, critical temperature of a niobium film $T_{c\mathrm{Nb}} \approx 9$ K).

The detector was manufactured in a clean area of NUST MISIS using standard methods of thin-film technology [15]. At the first stage, a photoresistive mask was created on a dielectric substrate of high-resistance silicon ($\rho > 6\,\mathrm{k\Omega \cdot cm}$) with a thickness of 500 μm, onto which a film of superconducting hafnium with a thickness of 80 nm was deposited by magnetron sputtering. Then, $1 \times 3\,\mu$m micro bridges were formed using lift-off lithography. Next, a superconducting niobium film with a thickness of 100 nm was deposited using magnetron sputtering. After the creation of the photoresistive mask, plasma chemical etching of a niobium film in an atmosphere of a mixture of gases $CF_4 + O_2$ was carried out to form a resonator, transmission lines and an inductor. It has been experimentally established that the hafnium film is not subject to plasma chemical etching, probably due to spontaneous passivation of its surface (formation of a strong oxide layer).

Fig. 2 shows an image of an experimental chip obtained using an optical microscope.

3. Calculation of detector parameters and characteristics

To develope the topology (layout) of the detector, its parameters and characteristics, we did not use estimate calculations as above. An electromagnetic model representing a configuration of conductors is developed taking into account the desired frequency band of the signal and the frequency of the resonator, as close as possible to the real device, implementing all these parameters in the AWR Design Environment software package [16]. The simulation allowed determining the optimal geometric dimensions of the device elements, such as the length of the resonator (19.6 mm), the width of the transmission lines of the detector resonator with an impedance of 50 Ω (the widthd of the strips is 20 μm, gap is 10 μm) and the length of the capacitive coupling of the resonator with the excitation line (700 μm). The frequency characteristics of the device for the carrier 1.5 GHz, excitation power of -90 dBm, resonator Q-factor $\sim 10^4$ were also calculated. As an example, the level of interference leakage from the detector carrier circuit into the signal circuit at the frequency of 7 GHz was estimated, which turned out to be less than -130 dBm. The detector operational depth of the suppression in the carrier circuit was $|S21| = -6$ dB, which corresponds to the optimal response efficiency of the resonator. It should be noted that, unlike the simplified equivalent circuit in Fig. 1, where the relative position of bridges and inductors is shown conditionally, the bridges are installed in the signal current line, which is necessary for minimal phase shift along the signal line between the bridges. At the same time, the inductors, which have significant geometric dimensions, are set aside, which does not contradict the original concept.

Let us turn to the problem of suppressing the pump signal of the detector in the useful signal circuit. It is clear that a violation of symmetry in the structure of the detector's absorbers, their inductive shunts, and the resonator itself adversely affects the balance (mutual subtraction) of currents and voltages in the signal circuit. However, there is a fundamental limit that arises due to the spatial diversity of the absorbers, which is equivalent to the mutual phase delay of two coherent sources of equal amplitude along the transmitting signal line. In this particular structure, the distance between the bridges is about $L \approx 7.5\,\mu$m, which corresponds to the phase shift of $\Delta\varphi = 2\pi L/\lambda$, and it is about $4 \cdot 10^{-4}$ rad at a resonator frequency of 1.5 GHz. It is the presence of such a phase shift that distinguishes the ideal (lumped-element) balanced scheme from the real one. An important factor is the difference in the inductance of the shunts and the resistance of the bridges, caused by the imperfection of the process of manufacturing of these elements. The electromagnetic analysis showed that a 10% deviation for bridges with ideal shunts creates a leakage of about -60 dB, and the simultaneous deviation of bridges and shunts gives an increase to -40 dB, which is comparable to the fundamental limit determined by spatial offset of the bridges. These figures are very small, despite significant

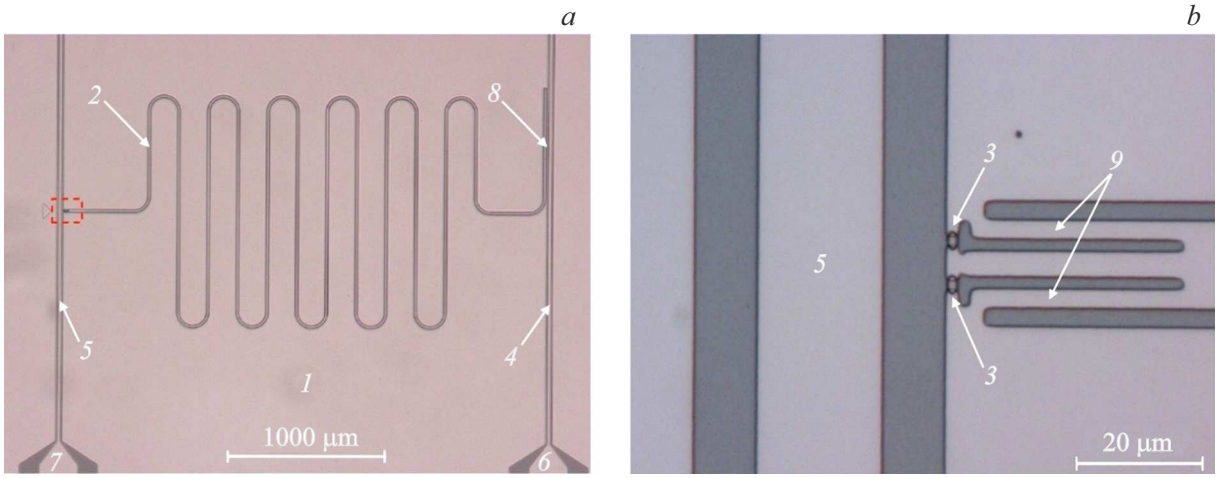

Figure 2. *a* — photo of the experimental chip obtained using an optical microscope, general view of the detector structure; *b* — enlarged area with superconducting bridges, outlined in Fig. 2, *a* by a dotted red line. The numbers of the element designations correspond to the diagram in Fig. 1, *a*.

deviations, which are greatly exaggerated for shunts. The expected deviations will be no more than 1–2%, which results in leakage at the level of −58 dB. The decrease in the effect of imbalance is attributable to the well-known effect of negative thermal feedback, which not only sets the voltage on the bridges, regardless of their impedance, but also redistributes the current in two loads connected to a coplanar resonator. Thus, the expected levels of pump signal suppression are sufficient for the current research goals (performance testing) of the new minimally invasive detection technology. The authors urge not to confuse the principle of invasive measurement of the Q-factor of the detector resonator, when the optimal level of heating of the nonlinear resistor is selected, and the penetration (invasion) of the carrier into the channel of the broadband signal being measured — such invasion is small.

4. Experiment

In the experimental part of the study, measurements of parameters |S21| (readout) and S41 (leakage) were carried out depending on the frequency and power of the pump (carrier) detectors in the line *4* (Fig. 1, *a*) and the power of the measured signal supplied to the transmission line *5*. The experimental setup included the following elements: a Triton DR-200 dilution cryostat (Oxford Instruments), a vector analyzer for measuring S-parameters (VNA, Vector Network Analyzer), a signal generator (AnaPico RFSG20), a low-noise cooled amplifier with a gain of 26 dB at a frequency of 1.5 GHz with noise of the order of 6 K, installed on stage 3 K, cold attenuators for suppressing background thermal noise 300 K (10 dB on stage 3 K and 20 dB on stage 50 mK).

The measured chip was installed in a holder equipped with microwave connectors of the SMP 40 type, to which signals from the generator and the S-parameter meter were supplied via coaxial superconducting cables. Further, these signals were transmitted along coplanar lines made on a printed circuit board; contacts to the chip were made using ultrasonic bonding to the pads *6* (Fig. 1, *a*) for the detector and to the contacts *7* for the signal. These four input/output ports of the microwave signal were designated as follows in the calculations: 1 and 2 ports — for exciting and reading the bolometer at a frequency of 1.5 GHz (contact pads *6*); *3* and *4* ports — for a passing signal at a frequency of 7 GHz (contact pads *7*). A VNA microwave signal was applied to the contact *6* of the detector's reading line at a detector resonator frequency of 1.5 GHz with attenuation of −36 dB, which was amplified by a 26 dB cooled amplifier from the chip output. The 7 GHz signal was applied to the chip contact *7* via a 30 dB cold attenuator from the microwave generator. The 20 dB cold attenuator was also connected to the signal line to isolate it from the background thermal noise at the output from the chip. The vector circuit analyzer (Agilent N5242A) recorded the transmission parameters of the circuit |S21(F)| and |S41(F)|.

The measurements were performed at a temperature of 130 mK. This temperature was chosen due to the insufficient reserve of thermal power of the refrigerator at lower temperatures due to the heating effect caused by the absiorbing (scattering) attenuators at 7 GHz. Additional studies are required to clarify the temperature range at which the target detector performance will be observed. As for classical RFTES, the optimal temperature of the electronic subsystem is near T_c, which should not be too high.

Fig. 3 shows a graph of the detector's response to changes in the power and frequency of the generator signal at a temperature of 130 mK and the optimal power level in the detector's pumping line. The abrupt response from the frequency with a period of about 0.66 GHz (individual points) most likely indicates the presence of a

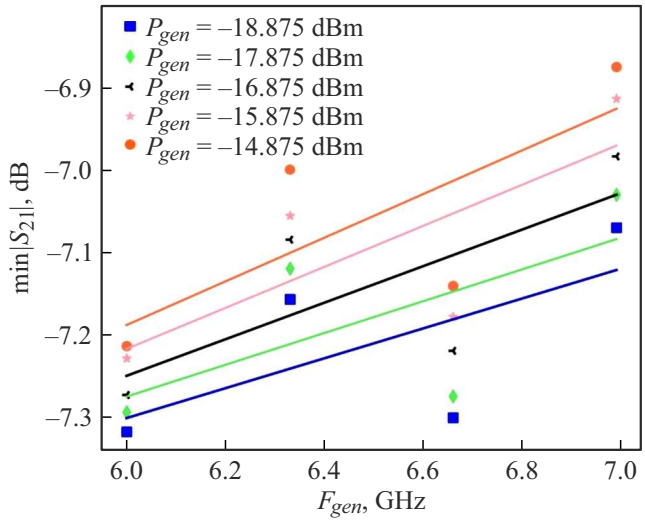

Figure 3. Dependence of the detector output signal (transmission level $|S21(F, P_{gen})|_{\min}$) on the frequency and power of the generator signal. Points — experimental data; solid lines — least squares fitting. The data provided comprise a calibration of the detector response. The calibration accuracy based on the standing wave is ±0.2 dB in the frequency range of 6–7 GHz.

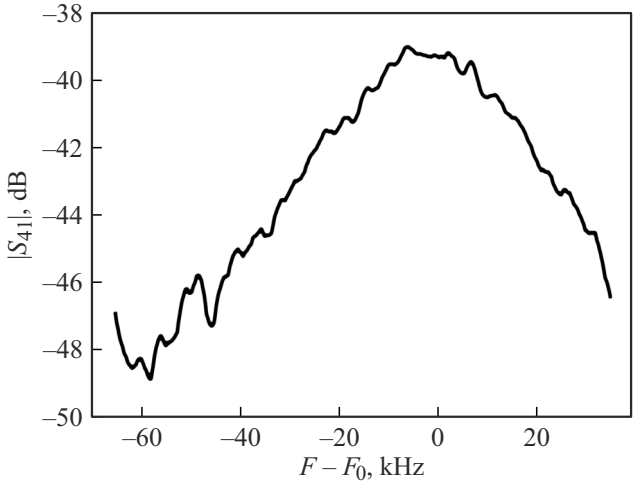

Figure 4. Amplitude-frequency response of the resonator |S41(F)| in the band of 100 kHz near the frequency of the resonator F_0. The parameter |S41(F)| indicates the level of leakage of the carrier into the signal circuit at the resonator resonance frequency of $F_0 = 1.5$ GHz. The noise level of the curve is explained by a weak signal caused by cold attenuators. A cooled amplifier was not used in this experiment.

small (0.3 dB) standing wave in the cold line of 6–7 GHz signal. Electromagnetic modeling has shown that such a deviation can be caused by inhomogeneities at the ends of a connecting coaxial cable with a length of ∼ 155 mm. This corresponds qualitatively to the experimental conditions regarding the chip connection, where a thermocompression connection (bonding) with ∼ 0.3 nH parasitic inductance on the chip side is used. An increase in frequency response is predictable due to an increase in the impedance of the inductors *9* (Fig. 1), which was discussed above in terms of the level of absorbed signal power. The power of the excitation/readout signal from the VNA, P_{in}, applied to the chip, varied within $P_{in} = 2, 4, \ldots 46$ nW. The approximation of the experimental data was obtained using linear regression.

Parameter |S41| describes the power transfer from the excitation line (port 1) to the signal line (port 4) and shows the level of carrier leakage into the signal circuit. The level of suppression of the detector carrier at a frequency of 1.5 GHz was measured directly using VNA and amounted to about −40 dB, as shown in Fig. 4, which indicates a good agreement with the above estimates. It should be noted that the carrier leakage into the signal line occurs only at a fixed detector polling frequency of 1.5 GHz within the measured band of 100 kHz. The interference in the frequency range of 6–7 GHz was not measured, as the sensitivity of the setup turned out to be below the level of this signal. The suppression at a frequency of 7 GHz should be at least 90 dB according to calculations.

Fig. 5 shows data on an unusually steep dependence of the transmission parameter |S21| on the power of the VNA (pumping) and the generator at a frequency of 6–7GHz (signal) at a temperature of 130 mK, which is similar to a temperature hysteresis, the origin of which is currently unclear: the resonator can switch between two ohmic loss states with a minimum frequency shift of the resonator in the range of such a jump, as shown in Fig. 5, *a*. To analyze this effect, a narrow area was selected from the scanning range, in which a jump of about 0.5dB (∼ 10 %) of the carrier power is displayed in the center of the resonator band. Experimental data obtained in a wider range of parameters indicate that there is a slight nonlinearity of kinetic inductance in the resonator of the detector (frequency shift of the resonator), as well as a smooth predictable increase in losses (expected resistive response). This is illustrated by experimental data |S21| (Fig. 5, *a*), the result of processing of which is shown in Fig. 5, *b*. Based on the thermal nature of the response, it is reasonable to conclude that the jump occurs at the same thermal power released on a nonlinear element, i.e., the sum of the pumping power and the signal is an invariant in the jump region. This allows writing the heat balance equation as follows:

$$P_{inv} = P_{gen}A + P_{in}B = \text{const},$$

where P_{inv} is the invariant of absorbed thermal power in the jump region, P_{gen} is the signal generator power, A is the signal absorption coefficient by bridges, P_{in} is the VNA power applied to the input of the chip. The depth of dip S21 = 6–7 dB means that the resonator load is close to the full matching mode, i.e. about 50 % (−3 dB) of the power supplied to the read line input, and $B \approx 0.5$. Solving the equation for $P_{inv} = 2.7 \cdot 10^{-8}$ W allows calculating the absorption coefficient $A = (-34.7 \pm 1.9)$ dB, which is in

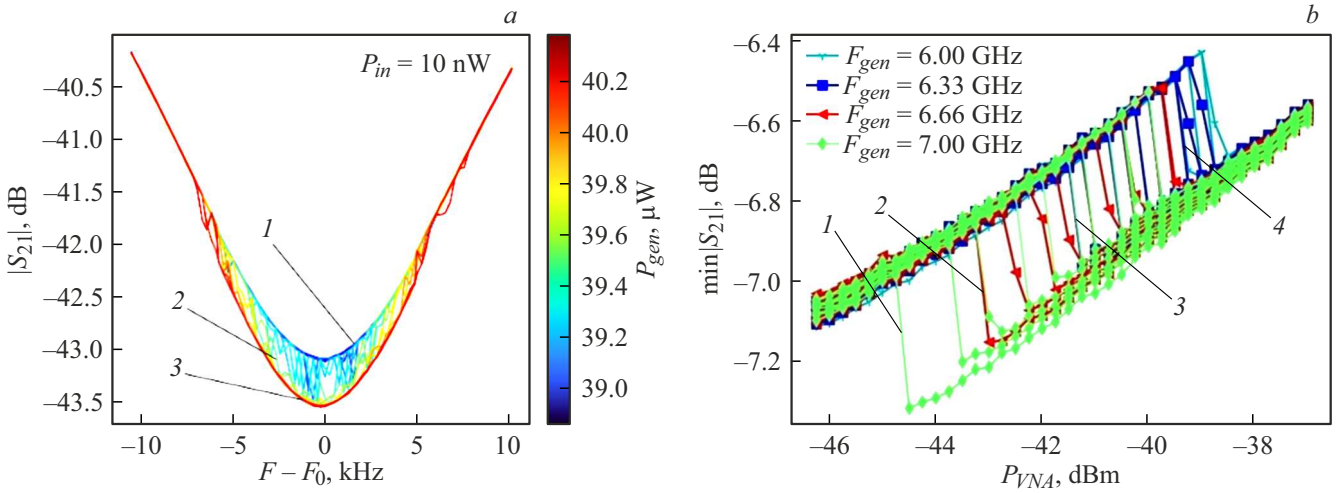

Figure 5. Experimental data on the response of the detector to heating by the sum of the powers of the measured signal and pumping. *a* — frequency dependences of the transmission parameter $|S21(F, P_{in}, P_{gen})|$ in a narrow range of pumping power for different strengths of 7 GHz signal at a temperature of 130 mK. The numbers on the graph indicate the signal ranges: *1* — 39.0–39.3 μW, *2* — 39.3–39.8 μW, *3* —39.8–40.2 μW; *b* — the dip depth depends on the pump power applied to the chip input and the signal power from −19 to −14 dBm (7–20 μW) at different oscillator frequencies. The numbers on the graph *b* indicate jumps |S21| for different frequencies of signal F_{gen}: *1* — 7, *2* — 6.66, *3* — 6.33, *4* — 6 GHz. F_0 — resonator frequency.

good agreement with the values of the model calculations (−34 dB) given above.

The abrapt variations (jumps) of |S21| is difficult to explain by the stationary properties of the system,since, assuming a resonant origin and taking into account that the frequency range of the jumps is less than 1 kHz, we obtain a Q-factor of resonances of more than 10^6. This seems unlikely in a system that is too short and damped at all ports with attenuators. Most likely, we are dealing with a combination of regular (smooth) detector response modes and dynamically unstable states. These states may have different physical natures. Instability can be associated with a change in the sign of the electrothermal feedback, and transitions are initiated by fluctuations (noises). This effect may also be related to (triggered by) the redistribution of energy between the parasitic electromagnetic modes of the chip, which was observed in electromagnetic modeling, and will be investigated in more detail later. Taking into account the lack of protection from the magnetic field in the experiment, the well-known effect of superconducting weak links (residual superconductivity in bridges) and inductive loops forming a kind of RF SQUIDs, where Josephson vortices can penetrate, should not be excluded [17].

Conclusion

The results of the development and preliminary tests of a transmission power detector based on RFTES technology at frequencies of 1.5 and 6–7GHz at a temperature of 130mK show that the developed principles and approaches are implemented experimentally with reasonable accuracy, and this detection technology at low gigahertz frequencies at ultra-low temperatures it deserves further, more detailed development. The measurement technique for such weak signals should be improved in terms of the signal-to-noise ratio using a second amplifier in the test signal circuit, as well as in the direction of expanding the range of input frequencies being tested. The discovered new unusual effect of the bistable state should be studied in more detail, since it can be based on both new effects of relaxation of films with an electron gas and parasitic resonant phenomena, for example, interference of the detector resonator with interconnecting circuits, or their mutual action, as well as the effects of local suppression of superconductivity inherent in double-bonded (having a hole) superconductors with weak links.

The experimentally measured Q-factor of the detector's reading circuit was about $4 \cdot 10^4$ at a carrier frequency of 1.55 GHz, which is in good agreement with model calculations. The depth of the detector's pump stop-band (suppression of power leakage at a frequency of 1.5 GHz into the signal circuit) is about −40 dB, which corresponds to numerical estimates and indicates a minor and predictable effect of the carrier on the signal line. A similar interference in the frequency range of 6–7 GHz turned out to be beyond the sensitivity limits of the system, and its measurement will require improvement of the experimental setup, which is important for determining the prospects of a new detector, in particular, in the field of reading the state of superconducting qubits. In summary, we would like to note that the proposed device looks useful for applications in radiometry and other fields where measurement of ultra-small signals under cryogenic conditions is required.

Acknowledgments

The authors are grateful to I.S.Besedin for a useful discussion.

Funding

The research was supported by a grant from the Russian Science Foundation 24-29-20298„Active Terahertz RFTES Detector“.

Conflict of interest

The authors declare that they have no conflict of interest.

References

[1] T.M. Lanting, H.-M. Cho, J. Clarke, M. Dobbs, A.T. Lee, P.L. Richards, H. Spieler, A. Smith. SPIE, **4855**, 172 (2003). DOI: 10.1117/12.459672
[2] J.J.A. Baselmans, J. Bueno, S.J.C. Yates, O. Yurduseven, N. Llombart, K. Karatsu, A.M. Baryshev, L. Ferrari, A. Endo, D.J. Thoen, P.J. de Visser1, R.M.J. Janssen, V. Murugesan, E.F.C. Driessen, G. Coiffard, J. Martin-Pintado, P. Hargrave, M. Griffin. Astronomy & Astrophysics, **601**, A89 (2017). DOI: 10.1051/0004-6361/201629653
[3] B.S. Karasik, A.V. Sergeev, D.E. Prober. IEEE Transactions on Terahertz Sci. Technol., **1** (1), 97 (2011). DOI: 10.1109/TTHZ.2011.2159560
[4] V.P. Koshelets, S.V. Shitov. Supercond. Sci. Technol., **13** (5), R53 (2000). DOI: 10.1088/0953-2048/13/5/201
[5] A.V. Merenkov, T.M. Kim, V.I. Chichkov, S.V. Kalinkin, S.V. Shitov. FTT, **64** (10), 1404 (2022) (in Russian). DOI: 10.21883/FTT.2022.10.53081.50HHC
[6] A.M. Gunyhó, S. Kundu, J. Ma, W. Liu, S. Niemelä, G. Catto, V. Vadimov, V. Vesterinen, P. Singh, Q. Chen, M. Möttönen. Nature Electron., **7** (4), 288 (2024). DOI: 10.1038/s41928-024-01147-7
[7] A. Opremcak, I.V. Pechenezhskiy, C. Howington, B.G. Christensen, M.A. Beck, E. Leonard Jr., J. Suttle, C. Wilen, K.N. Nesterov, G.J. Ribeill, T. Thorbeck, F. Schlenker, M.G. Vavilov, B.L.T. Plourde, R. McDermott. Science, **361** (6408), 1239 (2018). DOI: 10.1126/science.aat4625
[8] L. Bisigello, S.J.C. Yates, L. Ferrari, J.J.A. Baselmans, A. Baryshev. SPIE, **9914**, 913 (2016). DOI: 10.1117/12.2238643
[9] M. De Lucia, G. Ulbricht, E. Baldwin, J.D. Piercy, O. Creaner, C. Bracken, T.P. Ray. AIP Adv., **13** (12), (2023). DOI: 10.1063/5.0168365
[10] M. De Lucia, P. Dal Bo, E. Di Giorgi, T. Lari, C. Puglia, F. Paolucci. Instruments, **8** (4), 47 (2024). DOI: 10.3390/instruments8040047
[11] A.S. Zagorodny. *Izmeriteli moshchnosti signalov SVCH i KVCH diapazonov na osnove diodnyh detektorov* (Avtoref. kand. diss., TUSUR, Tomsk, 2014) (in Russian). https://rusneb.ru/catalog/000199_000009_005556707/
[12] S.V. Shitov, T.M. Kim, L.S. Solomatov, N.Yu. Rudenko, A.V. Merenkov, An.B. Ermakov, V.I. Chichkov. Technical Physics, **69** (7), 987 (2024). DOI: 10.61011/TP.2024.07.58802.168-24
[13] A.V. Merenkov, V.I. Chichkov, A.B. Ermakov, A.V. Ustinov, S.V. Shitov. IEEE Transactions on Appl. Superconduct., **28** (7), 1 (2018). DOI: 10.1109/TASC.2018.2827981
[14] M.E. Gershenson, D. Gong, T. Sato, B.S. Karasik, A.V. Sergeev. Appl. Phys. Lett., **79** (13), 2049 (2001). DOI: 10.1063/1.1407302
[15] A.I. Kurnosov, V.V. Yudin. *Tekhnologiya proizvodstva poluprovodnikovyh priborov i integral'nyh mikroskhem* (Vysshaya shkola, M., 1986) (in Russian).
[16] Cadence AWR Microwave Office https://www.awr.com/awr-software/products/awr-design-environment.
[17] P. Jung, S. Butz, M. Marthaler, M.V. Fistul, J. Leppäkangas, V.P. Koshelets, A.V. Ustinov. Nature Commun.0, **5** (1), 3730 (2014). DOI: 10.1038/ncomms4730

Translated by A.Akhtyamov